FEATURE ARTICLE

Multiphoton Control of the 1,3-Cyclohexadiene Ring-Opening Reaction in the Presence of Competing Solvent Reactions

Elizabeth C. Carroll,[†] James L. White,[‡] Andrei C. Florean, Philip H. Bucksbaum,[‡] and Roseanne J. Sension*

FOCUS Center, University of Michigan, 450 Church Street, Ann Arbor, Michigan 48109-1040

Received: February 14, 2008; Revised Manuscript Received: April 20, 2008

Although physical chemistry has often concentrated on the observation and understanding of chemical systems, the defining characteristic of chemistry remains the direction and control of chemical reactivity. Optical control of molecular dynamics, and thus of chemical reactivity provides a path to use photon energy as a smart reagent in a chemical system. In this paper, we discuss recent research in this field in the context of our studies of the multiphoton optical control of the photo-initiated ring-opening reaction of 1,3-cyclohexadiene (CHD) to form 1,3,5-*cis*-hexatriene (Z-HT). Closed-loop feedback and learning algorithms are able to identify pulses that increase the desired target state by as much as a factor of two. Mechanisms for control are discussed through the influence of the intensity dependence, the nonlinear power spectrum, and the projection of the pulses onto low orders of polynomial phase. Control measurements in neat solvents demonstrate that competing solvent fragmentation reactions must also be considered. In particular, multiphoton excitation of cyclohexane alone is capable of producing hexatriene. Statistical analyses of data sets obtained in learning algorithm searches in neat cyclohexane and for CHD in hexane and cyclohexane highlight the importance of linear and quadratic chirp, while demonstrating that the control features are not so easily defined. Higher order phase components are also important. On the basis of these results the involvement of low-frequency ground-state vibrational modes is proposed. When the population is transferred to the excited state, momentum along the torsional coordinate may keep the wave packet localized as it moves toward the conical intersections controlling the yield of Z-HT.

I. Introduction

The development of flexible, tunable ultrafast laser sources has led to an ever increasing flood of information elucidating chemical reaction dynamics. Ultrafast spectroscopic investigations have exploited the time resolution available with short pulses to probe the dynamics of molecular systems with ever increasing precision and sophistication. Multidimensional spectroscopies, both vibrational and electronic, are proving to be powerful tools to unravel the interplay between environment, structure, dynamics, and coherence.[1] The data obtained from these experiments serve as the foundation for the development of a unified picture of energy relaxation, energy redistribution, charge redistribution, atomic rearrangement, and other properties inherent to chemical reactivity.

But chemistry is not limited to observation and understanding. The overarching goal and defining characteristic of the discipline remains the direction and control of chemical reactivity. Optical control of molecular dynamics, and thus of chemical reactivity, has been actively pursued for many years. Early attempts using state selection generally failed as energy redistribution randomized the available energy on a time scale much faster than the time scale required for reaction to occur.[2] The development of ultrafast laser technologies capable of producing ultrashort broadband optical pulses has opened a new pathway for the control of chemical systems, bypassing many of the limitations imposed by energy randomization. Ultrashort broadband optical pulses may be temporally and spectrally manipulated using commercially produced pulse shapers.[3,4] The resulting "sculpted" pulses may be used as smart reagents to control molecular dynamics and chemical reactivity.[5–8]

The central challenge for the optical control of complex reactive systems is identifying control fields capable of achieving the desired target state. Even a molecule as small as cyclohexadiene, the system used in our investigations,[9] is large enough to prohibit sufficiently accurate electronic structure calculations while taking into account all vibrational degrees of freedom. Add to this the influence of a solvent bath on the dynamics and decoherence, and the calculation is intractable at the present time.

In this article we will outline the current state of the field of coherent control of chemical reactions in solution, concentrating on the use of feedback search methods to affect and interpret the optical control of reaction dynamics. This discussion is driven by analysis of experiments using feedback optimization to control the ring-opening reaction of 1,3-cyclohexadiene (CHD) to produce 1,3,5-*cis*-hexatriene. Multiphoton initiation of a photochemical reaction represents a subset of the active enterprise engaged in using pulse sculpting to probe or control

* Corresponding author. E-mail: rsension@umich.edu.
[†] Present address: University of California, Davis, CA.
[‡] Present address: Stanford University, Stanford, CA 94305.

10.1021/jp8013404 CCC: $40.75
Published on Web 07/01/2008

Elizabeth C. Carroll is currently a postdoctoral research fellow at the University of California, Davis. She received her Ph.D. in Applied Physics from the University of Michigan in 2006 for work on coherent control in ultrafast solution phase chemistry.

James L. White received his bachelor's degree from the University of Michigan in Physics and is currently a graduate student in Applied Physics at Stanford University. His research focuses on the use of statistical methods to analyze data sets obtained in optical control experiments and to use this analysis to extract mechanistic insight.

Andrei C. Florean is currently a Senior Scientist with Spectra Physics Lasers. He received his bachelor's degree in Physics from University of Bucharest, Romania, and his Ph.D. in Physics, from the University of Michigan in 2008 working on coherent control of quantum systems in liquid phase.

Philip H. Bucksbaum is Director of the PULSE Center at SLAC and Professor of Physics, Applied Physics, and Photon Science at Stanford University. He received his bachelor's degree from Harvard in 1975 and his Ph.D. in AMO Physics from the University of California, Berkeley, in 1980. He held appointments at Bell Laboratories and the University of Michigan before joining Stanford. His research interest is fundamental light-matter interactions, and especially the control of quantum systems using ultrafast laser fields. His group develops and uses new sources of ultrafast laser light in the infrared, visible, ultraviolet, and X-ray regions of the light spectrum.

Roseanne J. Sension is Professor of Chemistry and Physics at the University of Michigan. She received her bachelor's degree in Chemistry and Mathematics from Bethel College in St. Paul in 1981 and her Ph.D. in Chemistry from the University of California, Berkeley, in 1986. She has been on the faculty at Michigan since 1992. Her research interests include the use of state-of-the-art ultrafast lasers and spectroscopic techniques to observe and control photoinitiated reactions.

molecular systems. This article will not explicitly consider the equally important work being pursued to use feedback and optical pulse shaping to identify pulses capable of enhancing spectroscopic signatures for chemical identification, weak field control of molecular dynamics, or the ongoing efforts to use systematic searches to identify optimal pulses for optical control or molecular spectroscopy.

A. Searching for Optimal Pulses. One approach to finding an appropriate control field is to recast the molecular dynamics problem as an optimization problem. Theoretical applications of optimal control theory (OCT) involve optimizing the transition probability from an initial state to the target state.[5,7] Still, it may not be possible to calculate the effect of a given field in a reasonable amount of time. On the other hand, experimentally, the reactive system itself can evaluate the efficacy of a given field "instantaneously".[7,8,10] This has led to the utilization of global search algorithms using the system to identify effective control fields. Stochastic optimization algorithms like the genetic algorithm can be used when the fitness landscape is complex and contains local maxima.

The goal of an adaptive feedback control experiment is to identify the parameters characteristic of an optical field capable of achieving control. In principle, the phase and amplitude of all the resolvable frequency components of the excitation pulse represents the set of control parameters. In most cases the size of the available parameter space prohibits an exhaustive search. One can sometimes use physical intuition to define an appropriate parameterization for the electric field and perform an exhaustive search to find the optimal field within that parameterization. If one does not want to make assumptions about the correct field parameterization, an alternative is to use a global search algorithm to attempt to identify sufficient pulse parameters. The standard practice in optimal control experiments is to use a learning algorithm based on the genetic algorithm (GA) guided by a feedback measurement to search the space of the control field. Judson and Rabitz first proposed application of genetic algorithm approaches to coherent control experiments.[7] The early strength of the method was demonstrated by Wilson, Warren, and coworkers[11] and by Gerber and coworkers,[12] as summarized by Levis and Rabitz.[10]

In a GA, candidate control fields are represented as a population of genomes, where each genome comprises phase or amplitude information for an optical pulse.[13] The algorithm encourages desirable traits in the gene pool by assessing the effectiveness of each pulse using a fitness function whose value is based on some measurement of the system reflecting the objective of the control experiment. In a set of sequential experiments, each genome is tested against the control objective and assigned a merit score, or fitness. The fittest genomes are used to produce the next population, or generation. Statistically, fit individuals have pulse characteristics that are either sufficient or necessary for survival. By "survival of the fittest", these traits eventually dominate the population. A refinement of the algorithm used to search the parameter space involves inclusion of an adaptive learning step that evaluates the relative success of the various mating and mutation operators at generating fit genomes; the use of each operator is weighted according to its past accomplishment.[13]

The termination criterion for the algorithm is somewhat arbitrary. In an ideal case the population would converge on a single optimal solution and searches beginning with different sets of initial pulses would converge to the same solution. In practice, due to the stochastic nature of the GA and experimental noise, different runs produce optimal pulses with similar features—and distinct "neutral" differences. The results of several searches must be analyzed to identify which traits in an optimal field are necessary and which are merely sufficient. Population size, mutation rate, and the specific operators used in mating all influence the rate of convergence, or even whether the algorithm will converge. Each of these factors should be optimized for convergence in each type of experiment.

The optimal pulses obtained in a learning algorithm search may be analyzed to determine common features responsible for control. However, there is no need to draw conclusions only from the limited number of optimal pulses obtained in separate experiments. Each GA search tests hundreds or thousands of different pulses shapes. Analysis of the entire set of trial pulses can help to determine the key features effective for control of a given system and to identify optimal basis sets for optical control of related systems.[9,14–19] In these experiments the search sets do not represent random samplings of pulses. Rather, these search sets are biased in the fitness-directed search. The bias in the search does not discredit statistical analysis of the search set but must be recognized in analysis of pulse characteristics and taken into account in the data interpretation.[16,18–21]

B. Cyclohexadiene Ring-Opening Reaction. 1,3-Cyclohexadiene (CHD) is considered a paradigm system for electrocyclic reactions[22–28] and constitutes the photo-active moiety in a number of important photochemical reactions, such as the formation of previtamin D from 7-dehydrocholesterol.[28–30] The ring closure reaction Z-HT → CHD has not been observed in the isolated CHD system, though both ring-opening and ring-closure reactions are readily observed in 7-dehydrocholesterol[29,30] and in photochromic fulgides[31,32] where the ring is sterically hindered. Fulgides have generated interest in the ultrafast chemistry community as potential photoswitches.[31]

The ring-opening reaction is illustrated in Figure 1. Although this schematic depicts only one generalized reaction coordinate, CHD has 36 degrees of freedom and the reaction dynamics are

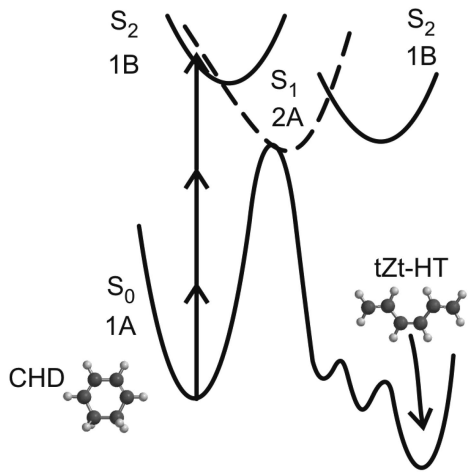

Figure 1. Schematic diagram of the CHD photochemical ring-opening reaction.

governed by multidimensional S_0, S_1, and S_2 potential energy surfaces (PES) that intersect to form conical intersections (CoIns). Conical intersections are particularly important in ultrafast photochemistry because they provide nonadiabatic photochemical decay channels which are often barrierless and lead to subpicosecond dynamics.

The single photon reaction scheme involves an ultraviolet transition between the ground electronic state and the antisymmetric (S_2) excited state. This excitation produces an electronic population and vibrational wave packet in the excited state. The wave packet accelerates along the torsional reaction coordinate[33] and passes through a CoIn to the 2A (S_1) excited state where most of the nuclear ring-opening dynamics occur. The electronic population returns to the ground state through internal conversion involving several CoIns between the 1A and 2A potential-energy surfaces[34–37] within a few hundred femtoseconds.[29] Sixty percent of the excited molecules relax to vibrationally excited CHD, and the remaining 40% convert to vibrationally and conformationally excited *cis*-1,3,5-hexatriene.[38]

At least two conical intersections connecting the S_1 and the S_0 potential energy surfaces of CHD are thought to contribute to the Z-HT yield. The CoIns represent different reaction pathways. Wave packet propagation studies by Hofmann and de Vivie-Riedle[39–41] demonstrated that following internal conversion from the S_2 state, the wave packet bifurcates on the S_1 PES and the reaction proceeds through both pathways.

The existence of multiple reaction paths, and the sensitivity of the wave packet bifurcation to initial conditions make CHD an attractive candidate for coherent control.[32,39–43] The resonant wave packet simulations used approximately 30000 cm^{-1} of coherent bandwidth to excite CHD; such broad bandwidth pulses are not available in the laboratory. Multiphoton excitation, on the other hand, may open control pathways not available to a one-photon resonance, such as multiphoton interference or direct excitation to the S_1 surface.

We recently reported[9] experiments demonstrating coherent control of the CHD ring-opening reaction with relatively narrow bandwidth 800 nm pulses ($\Delta\nu \leq 310$ cm^{-1}). In this excitation scheme, three-photon absorption is required to electronically excite CHD. Shaped pulses were identified that increased the yield of the CHD reaction by a factor of two over transform-limited 800 nm excitation. The highest yields of Z-HT occurred for pulses possessing substantial negative quadratic phase. In addition to the CHD reaction, however, side reactions were observed in the solvent.

In the present paper, we explore the role of the solvent in more detail. We contrast the quality of the solutions obtained in solvent and use an analysis of the full set of trial pulses to isolate key features effective for control and to identify optimal parameters for optical control of the ring-opening reaction.

II. Experimental Methods

In these experiments, a customized genetic algorithm[13] was used to search for the optimal pulse and the efficacy of each pulse was determined using the ultraviolet (UV) absorption spectrum. The experimental setup, described in detail earlier,[9] achieved control of the spectral phase of 800 nm, 50 fs laser pulses using a pulse shaping system based on a zero-dispersion Fourier filter design using an acousto-optic modulator (AOM).[4,44] The maximum intensity of the transform-limited pulse at the sample was estimated to be 1.8×10^{12} W/cm^2. Formation of the Z-HT photoproduct was probed using a UV continuum fixed at a time delay of either 1 or 12 ns following excitation. Differential absorption of the probe pulse provides a direct measure of the concentration of Z-HT created by the pump pulse in the excitation volume. The transmitted probe was collected with a multichannel spectrometer (Ocean Optics S2000), and the pump pulse was optically chopped to alternately obtain spectra with (I_{sig}) and without (I_{ref}) excitation. The difference spectrum $\Delta A(\lambda) = -\log[I_{sig}(\lambda)/I_{ref}(\lambda)]$ provides a direct measure of the concentration of Z-HT produced by the excitation pulse, and was used to evaluate fitness in the learning algorithm. Generally, 10−30 pumped/unpumped pairs were collected, each with an integration time of 50 ms, so the transient difference spectrum ΔA represents the average of at least 1000 laser pulses. Two feedback goals were used: goal 1 optimized for the maximum absorption between 260 and 280 nm; goal 2 optimized for the maximum absorption between 260 nm and 280 nm and added a penalty for absorption between 280 nm and 300 nm where Z-HT does not absorb.[9] The latter goal was designed to discriminate against solvent side reactions.

Samples were prepared by diluting 1,3-cyclohexadiene (Aldrich) with either spectroscopic grade cyclohexane or hexane. The sample, with an optical density of approximately 1 at 266 nm, was flowed though a 1 mm thick quartz flow cell at a rate sufficient to replenish the sample between laser pulses. A 100 mL sample reservoir was used to prevent the buildup of photoproducts in the bulk sample. Control experiments were also performed using samples of neat solvent. These data were subjected to the same analysis as the data obtained using CHD samples.

III. Results

Excitation of CHD in either hexane or cyclohexane with transform-limited 800 nm pulses resulted in the formation of Z-HT. The presence of the Z-HT photoproduct was confirmed in both the transient difference spectrum and in the steady-state UV absorption spectrum of a sample irradiated in a small volume flow cell to allow photoproduct accumulation.[9] As described in our earlier report,[9] shaped pulses were identified that increased the yield of the CHD reaction by a factor of two over transform-limited 800 nm excitation. The highest yields of Z-HT occurred for pulses possessing substantial negative quadratic phase. Steady-state spectra of all samples also exhibited strong absorption in the deep UV ($\lambda < 240$ nm) due to solvent photodissociation photoproducts.[9]

A. Identifying Solvent Involvement in Feedback Control. The difference spectrum observed following multiphoton excitation of CHD samples at 800 nm is complicated by the presence

of a broad positive background absorption spanning the probe spectrum.[9] A similar broad difference spectrum is observed following multiphoton excitation of neat solvent. From these data it was concluded that the difference spectrum observed in the CHD solution contains two components: (1) Z-HT produced from CHD, and (2) a transient signal consistent with excitation and fragmentation of the solvent. The difference spectra obtained following multiphoton excitation were fit to a linear combination of the background solvent spectrum and the steady-state Z-HT-CHD difference spectrum:

$$\Delta A(\lambda) = c_1 \Delta A_{\text{solvent}}(\lambda) + c_2 \Delta A_{\text{HT-CHD}}(\lambda) \quad (1)$$

The solvent contribution observed between 260 and 300 nm was found to be transient on a nanosecond timescale.[9] $\Delta A_{\text{HT-CHD}}(\lambda)$ corresponds to formation of a stable photoproduct and is constant after the ring-opening reaction is complete ($\ll$100 ps under linear excitation conditions[24–27]). Given the different dynamics of these two signals, optimization experiments probing the solution at longer time delay will be influenced more by the CHD → Z-HT reaction than by the solvent processes. Consequently, the difference spectrum was optimized at two delay times (τ = 1, 12 ns) to distinguish the transient contribution of the solvent processes from the steady-state contribution of Z-HT formation.

Our original analysis of multiphoton optical control in CHD[9] assumed that the solvent transient spectrum did not vary with pulse shape. This assumption does not always hold. To make a more accurate separation of the contributions of solvent background and Z-HT formation, we used the data obtained through GA optimization of the signal in neat solvent at each time delay using goal 1 as the fitness function. Optimized solvent spectra were generated by singular value decomposition[45] of the set of highest-fitness spectra from each generation of the GA. These spectra are used to analyze the data obtained from GA optimization of the CHD → Z-HT reaction in hexane and in cyclohexane.

i. CHD/Hexane. In hexane, the most significant basis spectrum differed slightly from the solvent spectrum produced by the TL pulse. The spectrum in hexane decreased in magnitude between τ = 1 and 12 ns, but there was no significant evolution in the spectral features. When the optimized solvent spectra were used to analyze the data, the remaining absorption contribution closely matches the Z-HT spectrum. The results from two experiments at each probe delay are plotted in Figure 2.

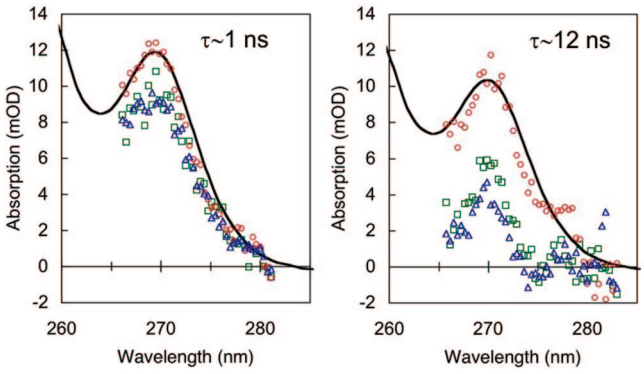

Figure 2. Change in absorption attributed to the formation of Z-HT in hexane with the background contribution subtracted. Blue triangles: data obtained with transform limited pulses. Red circles: data obtained with optimal pulses in a search driven by feedback goal 1. Green squares: data obtained with optimal pulses in a search driven by feedback goal 2. The black line represents the target spectrum for the formation of Z-HT from CHD. Probe delays are indicated.

The changes in solvent and Z-HT contributions, relative to the TL pulse, were calculated using both the TL solvent spectrum and the optimized solvent spectrum. These data are summarized in Table 1. Although the precise form of the solvent spectrum affects the perceived change in yield, the results from both procedures are in qualitative agreement. The actual values likely lie within the range of the fit parameters derived from the two solvent spectra. At τ = 1 ns, the optimal pulse obtained for goal 1 substantially increased Z-HT (40−100%), and the solvent background signal increased by ca. 10%. Goal 2 resulted in a substantial suppression of the solvent background, and left the Z-HT signal essentially unchanged. Optimization at τ = 12 ns resulted in a substantial increase in Z-HT signal for both feedback goals. However, goal 2 was not effective in suppressing the solvent signal at this longer delay.

ii. CHD/Cyclohexane. It was observed earlier that the targeted photoproduct, Z-HT, could be produced from a highly nonlinear interaction with neat cyclohexane[9] adding a contribution, $\Delta A_{\text{Z-HT}}(\lambda)$, to the observed signal:

$$\Delta A(\lambda) = c_1 \Delta A_{\text{solvent}}(\lambda) + c_2 \Delta A_{\text{HT-CHD}}(\lambda) + c_3 A_{\text{Z-HT}}(\lambda) \quad (2)$$

GA searches were able to improve the signal, but it was not possible to distinguish between contributions from the solvent and CHD in the feedback measurement; at τ = 1 ns the difference spectrum observed in the CHD solution and neat cyclohexane were nearly identical. Still, it was reasoned that the GA searches conducted at the longer time delay would be influenced less by the solvent processes, and would better reflect the target CHD → Z-HT reaction. At τ = 12 ns, the difference spectrum exhibited absorption characteristics of Z-HT. Some of these results were originally reported with our CHD/hexane results.[9] Separate analysis of these pulse shapes is included below.

B. Identification of Control Parameters. The data described above illustrate the optimization of the production of Z-HT from CHD through multiphoton interaction with 800 nm pulses. In this section the correlations between pulse characteristics and pulse performance are systematically analyzed for the hundreds of different pulses tested during the course of each GA search. Duplicate pulses, which were tested multiple times, were removed from the search sets and represented by an average fitness. Even so, the search set does not represent a random sampling of pulses because the learning algorithm search is fitness-directed. It is common for the genomes in each generation become increasingly similar as the GA converges on a solution, although random mutation operations continually introduce new pulse features. Because of this bias the optimal solution will be weighted most heavily in analysis of pulse characteristics. In this sense, the search set provides information about the robustness of pulse parameters. The most robust pulse characteristics likely correspond to control parameters in the optimization experiment.

i. Intensity Dependence. These experiments rely on multiphoton absorption to initiate the CHD ring-opening, so pulse intensity is expected to be a dominant control parameter in optimizing Z-HT production. The probability for three-photon absorption scales as I^3. In our earlier report[9] the correlation between pulse fitness and integrated third-order nonlinear power, $P_{3\omega}$, was analyzed for two searches carried out for goal 1, where, $P_{3\omega} = \int S_3(\omega)\, d\omega$ and $S_3(\omega)$ is given by

$$S_3(\omega) = \left| \int\int d\Omega_1\, d\Omega_2\, A(\Omega_1)\, A(\Omega_2)\, A(\omega - \Omega_1 - \Omega_2) e^{i[\varphi(\Omega_1)+\varphi(\Omega_2)+\varphi(\omega-\Omega_1-\Omega_2)-\varphi_{TL}]} \right|^2 \quad (3)$$

This analysis demonstrated a weak but clear correlation between

TABLE 1: Percent Changes in the Z-HT and Solvent Contributions to the Transient Difference Spectrum, Relative to the Transform-Limited Pulse for Four GA Searches

		% change in signal			
		TL solvent spectrum		optimal solvent spectrum	
feedback goal	probe delay (ns)	solvent	Z-HT	solvent	Z-HT
1	1	+13	+100	+10	+40
2	1	−50	+5	−40	+5
1	12	+70	+180	+60	+150
2	12	+100	+150	+40	+90

pulse fitness and $P_{3\omega}$ when the probe is delayed by 1 ns, and no correlation when the probe is delayed by 12 ns.[9] Similar analysis including the GA runs using the goal 2 fitness function shows the same trend (Figure 3). The Z-HT absorption spectrum is constant on the nanosecond timescale, but the solvent transient decreases. Thus, the dependence of the intensity correlation on probe delay suggests that, at the early time delay, the solvent signal has more influence over the GA solution and the weak correlation of pulse fitness with third-order power is dominated by the interaction of the pulse with the solvent. At the later time delay, the Z-HT signal has greater contribution to the feedback signal and has the opportunity to guide the search away from the TL.

Several multiphoton experiments in the literature compensate for the intrinsic intensity dependence by taking the fitness as a ratio between two nonlinear processes of the same order.[46–48] The common dependence of the nonlinear processes on the integrated nonlinear power spectrum, $\int S_n(\omega)\, d\omega$, cancels in the ratio, leaving the fitness function dependent only on the properties of the molecular system under study. This method has proved useful in isolating small pulse-shape dependencies in experiments which would otherwise have discovered only the trivial result of a transform-limited pulse. In the present experiments, non-transform-limited pulses were found to be effective despite the intensity dependence. Because the feedback signal does not follow the expected intensity dependence, it is not clear whether normalizing by an I^3 dependent process would have improved the feedback sensitivity.

ii. Nonlinear Power Spectrum. The pulse bandwidth provides multiple n-photon combinations to satisfy a single molecular transition. Interference between components of the fundamental field effectively shapes the nonlinear power spectrum governing the dipole response of the molecular system. Meshulach and Silberberg showed the effect of shaping the nonlinear power spectrum for a narrow band transition in Cesium vapor.[49] In a more complex condensed phase system, Lozovoy et al.[50] demonstrated that nonlinear spectral filtering could be used to selectively excite a species in a mixture of dyes with similar absorption spectra. In this case, the nonlinear interaction creates a narrowband nonlinear filter tuned to the spectral region where the different species are most distinguishable.

The mechanism for control of Z-HT formation could simply represent an exploitation of frequency tuning in the third-order spectrum. We must also consider the possibility that the one-photon forbidden S_1 state is excited directly by three photon absorption. The formation of Z-HT could then be influenced by competition between the $S_0 \rightarrow S_1$ or $S_0 \rightarrow S_2$ excitation paths. Competition between excitation pathways could conceivably be observed if the nonlinear power spectrum is shaped to exploit differences in the S_1 and S_2 absorption spectra. Though the absorption bands for both excited states in the CHD system are broad, the S_1 spectrum is expected to be red-shifted.

We analyzed the degree of correlation between pulse fitness and power in the third harmonic frequency 3ω. When high fitness requires high $P_{3\omega}$, the correlation will approach 1. When

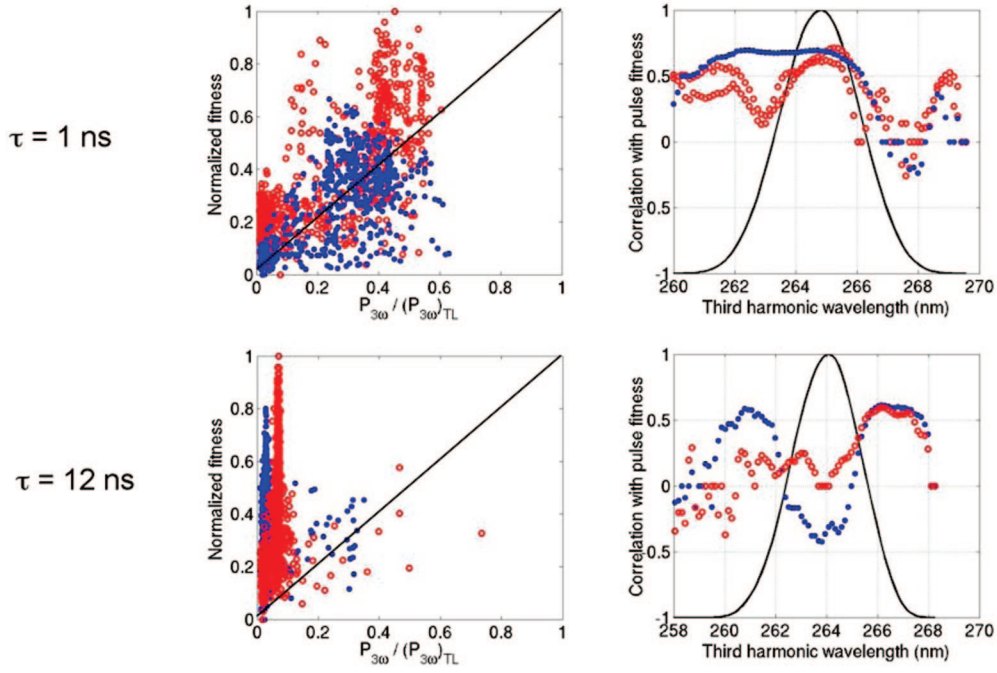

Figure 3. Left: correlation between normalized fitness and peak power. Right: correlation coefficients between third harmonic wavelength and pulse fitness. Goal 1 searches are marked in red. Goal 2 searches are marked in blue.

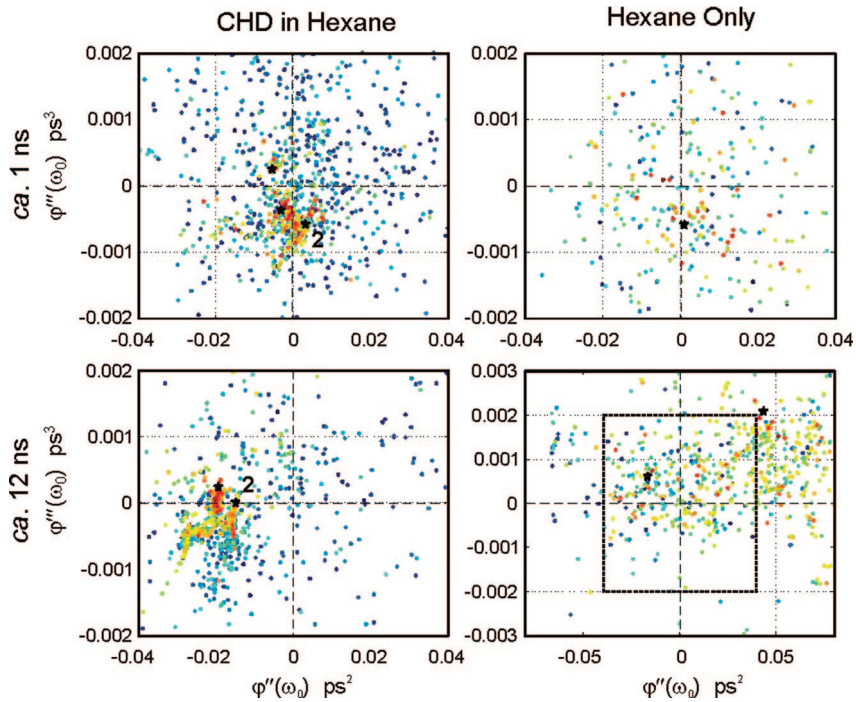

Figure 4. Two-dimensional fitness landscape parameterized in orders of chirp for CHD/hexane. Pulse fitness is compared with the projection of spectral phase onto linear and quadratic chirp. Fitness is indicated by color with red corresponding to high fitness and blue corresponding to low fitness. The number 2 next to a solution (black star) indicates the control goal 2 was used as a fitness function in the GA. Otherwise, the searches were optimized using control goal 1. The solvent-only search of hexane with a 12 ns probe delay sampled a much larger region of phase space. The dashed square corresponds to the space plotted in the other three maps.

high fitness requires low $P_{3\omega}$, the correlation will approach −1. The correlation coefficient c(x,y) was calculated as

$$c(x,y) = \frac{n\sum xy - \sum x \sum y}{\sqrt{(n\sum x^2 - (\sum x)^2)(n\sum y^2 - (\sum y)^2)}} \quad (4)$$

where $x = P_{3\omega}$, $y =$ fitness, and n is the number of points in the data set. The results are shown in Figure 3.

At 1 ns, there is a moderately high degree of correlation for most of the spectrum. The red edge of the 3ω spectrum has the lowest correlation. This correlation pattern is consistent with the solution having a relatively high peak power. The analysis of nonlinear power spectra shows no evidence that the GA is pressured toward pulses which produce narrow features in the nonlinear power spectrum. This is not surprising as all of the absorption features in solution are characterized by broad spectral bands. The bias toward the blue edge of the spectrum, apparent in three separate searches may also reflect a real preference for three photon absorption at higher frequencies, especially as the trend is more pronounced in the goal 2 search than in the two goal 1 searches.

In contrast, at 12 ns the highest correlation occurs in both wings of the spectrum. The middle of the 3ω spectrum has low correlation for goal 1 and is anti-correlated for goal 2. The latter pattern of correlation is consistent with a highly chirped solution, where the longer pulse duration reduces the peak power but preserves the spectral bandwidth. Still, it is not obvious whether the driving mechanism is minimizing the energy density in the middle of the spectrum or whether it is more important to distribute the energy in a particular way in time. The analysis of nonlinear power spectra again shows no evidence that the GA is pressured toward pulses which emphasize spectral features in the nonlinear power spectrum. Therefore it is unlikely that nonlinear spectral filtering plays an important role in the optimized multiphoton production of Z-HT from CHD.

iii. Chirp Subspace. In this section, we examine the phase relationships between frequencies in the fundamental shaped pulse. The results published earlier[9] suggested that negative linear chirp is a common feature among the pulses producing a higher Z-HT yield. To analyze the dependency on chirp in detail, we fit the phase of each pulse to a fourth-order polynomial and compared to the coefficients of a Taylor expansion of spectral phase:

$$\varphi(\omega) = \varphi(\omega_o) + \varphi'(\omega_o)(\omega - \omega_o) + \frac{1}{2!}\varphi''(\omega_o)(\omega - \omega_o)^2 + \frac{1}{3!}\varphi'''(\omega_o)(\omega - \omega_o)^3 + \ldots \quad (5)$$

The second- and third-order terms represent linear and quadratic chirp.

We found that the majority of pulses in each search set fit relatively well to a polynomial and that the pulses poorly modeled by a polynomial fit also corresponded to low fitness. The high incidence of smooth chirped solutions can be attributed in part to the choice of mating operations used in the GA. Three of the six operators used (smoothing, creep, and polynomial mutation) tend to produce pulses with smoother phase than the parent pulses. The polynomial mutation operator explicitly introduces segments of phase described by eq 3. In addition, the GA implements operator adaptation and the probability of operator selection is influenced by the operator's history of producing high-fitness pulses.[13]

In our earlier paper (in Figure 11[9]) we presented a plot that analyzed pulse fitness as a function of quadratic and cubic phase coefficients for a number of different searches. This analysis demonstrated the bias away from transform-limited pulses but failed to convey a true picture of the dependence of pulse fitness

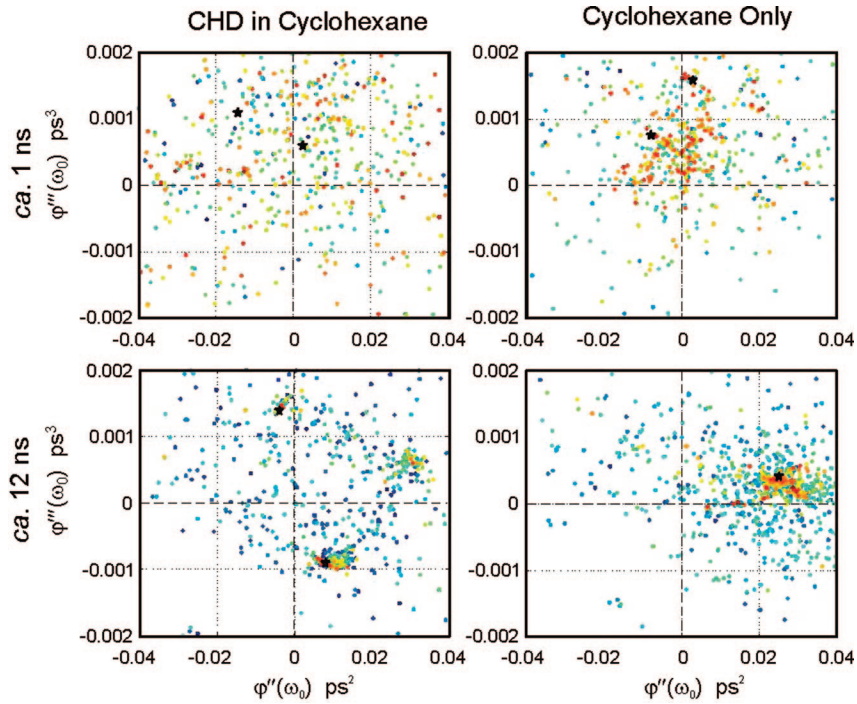

Figure 5. Two-dimensional fitness landscape parameterized in orders of chirp for CHD/cyclohexane. Pulse fitness is compared with the projection of spectral phase onto linear and quadratic chirp. Fitness is indicated by color with red corresponding to high fitness and blue corresponding to low fitness. The stars indicate optimal pulses identified in different GA searches, all carried out with feedback goal 1.

on the phase coefficients. Figure 4 shows fitness maps illustrating the distribution of fitness in the linear and quadratic chirp parameters for CHD in hexane and contrasts those maps with the fitness maps obtained for neat solvent.

There are several points of interest:

(1) In the CHD searches, the high-fitness pulses cluster around the optimal solutions. The chirp space is also most densely sampled around the optimal pulse. This demonstrates convergence of the GA searches in the chirp subspace. In neat hexane, high-fitness pulses are not clustered and the searches do not converge consistently. Although it is possible that the chirp subspace does not represent the "correct" control parameters for the solvent system, inspection of the programmed pulses also indicated that the GA searches converged poorly.

(2) Where other quadrants of the subspace were sampled, the fitness is low; e.g., positive chirp is not as effective in optimizing the Z-HT reaction. Evidently, the sign of chirp is important, indicating that the mechanism of control is not simply to reduce peak power or increase pulse duration.

(3) The solutions cluster in different regions of the chirp space at the two time delays. This was to be expected from analysis of the nonlinear spectrum and nonlinear power. We note that the spaces sampled at the two time delays are not the same. It is slightly problematic to compare the search spaces directly, as the projections onto linear and quadratic chirp do not fully represent the pulses. For instance, the searches at $\tau = 12$ ns show low-fitness behavior near the transform-limit, but it was seen in the nonlinear power analysis (Figure 3) that the GA did not really test any pulses with more than ~60% of the peak nonlinear power (corresponding to the TL pulse). Parameters outside this two-dimensional chirp subspace account for the low nonlinear power. Nonetheless, projection into the chirp space creates a common control parameter space where the CHD and solvent systems can be viewed together.

(4) The above analysis also provides a measure of how thoroughly the genetic algorithm searched the lower dimensional space spanned by the basis set: $[\omega^2, \omega^3, \omega^4]$. The GA is restricted to use only pulses where the maximum change in phase between two "pixels" is π, resulting in a maximum linear chirp of 8×10^4 fs^2; the maximum quadratic chirp allowed is 4×10^6 fs^3. Based on the ranges of chirp parameters derived from the polynomial fits, the GA searches sampled a significant amount of the chirp space.

iv. CHD in Cyclohexane. Optimization experiments similar to those described in CHD/hexane solutions were also performed on solutions of CHD and cyclohexane. Because in this system the highly nonlinear interaction with the solvent can lead to the target hexatriene photoproduct, the fitness landscapes of these searches are particularly informative and provide important insights into the optimization process.

Figure 5 shows fitness maps for the chirp subspace from the cyclohexane data, generated in the manner described above. At $\tau = 1$ ns, the high-fitness pulses are scattered and there is no convergence in the chirp parameters for the CHD/cyclohexane searches. The high-fitness pulses in neat cyclohexane cluster loosely around the TL. These fitness landscapes are consistent with a poorly defined problem. In contrast, at $\tau = 12$ ns GA searches converged for both CHD in cyclohexane and neat cyclohexane samples. In the CHD/cyclohexane solution, repeated searches did not converge to the same region of the chirp subspace. Searches in neat cyclohexane more consistently converged to large values of positive linear chirp and moderate values of positive quadratic chirp. This indicates that the feedback control loop optimized some process in cyclohexane. Steady-state measurements also demonstrated enhanced formation of HT from multiphoton excitation of cyclohexane, suggesting that the optimized process pertained to photodissociation events that led to HT formation.

An interesting feature among the $\tau = 12$ ns search sets is a cluster of high fitness emerging in the region of chirp space optimal for solvent processes. It appears that the GA simultaneously identifies both the CHD optimum and solvent optimum.

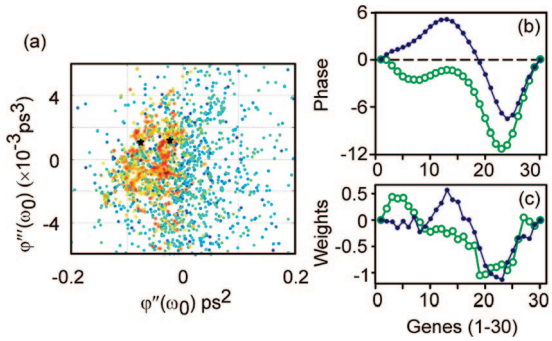

Figure 6. (a) Two-dimensional fitness landscape parameterized in orders of chirp for CHD/cyclohexane as described in Figure 5. These searches were carried out using narrow bandwidth (8 nm) pulses at a 10 Hz repetition rate. (b) Phase profiles of optimal pulses for two CHD experiments and (c) normalized most correlated feature (MCF) calculated for each experiment (color coordinated).

It is also interesting to note that the optimal pulse shapes identified for CHD in hexane and cyclohexane differ significantly, suggesting that the control mechanisms differ. In contrast, in an earlier narrowband study using 10 Hz, 800 nm pulses to excite CHD in cyclohexane also found negative chirp to be a significant component of the optimal solution.[9,21] In these experiments, the probe delay was greater than 12 ns and could have allowed greater temporal distinction between transient solvent processes and the CHD isomerization.

v. Principal Component Analysis of the Search Space. The best pulse shapes and the analyses above suggest that negative chirp is an important feature of the control pulses. To test this observation, a statistical analysis of the search set was performed to identify important features of the control pulses without assuming beforehand that low-order polynomial phase would constitute an appropriate basis. Principal component analysis (PCA) was used to identify a basis set for the search space ranked according to the variance of the pulses tested during the search.[18,51] The correlation of fitness with projection onto each principal component is then determined. A direction that has both a large variance and a substantial correlation with fitness is likely to be interesting. This is not necessarily true, however.[19] Thus the search space directions having the highest correlation with fitness, without regard to variance, are also calculated.[21]

This analysis was initially applied to data sets obtained in experiments where narrow bandwidth (ca. 8 nm), 10 Hz, 800 nm pulses were used to excite CHD in cyclohexane.[9,18,21] As observed for CHD in hexane, projection of the fitness space onto linear and quadratic chirp parameters highlights the importance of negative linear chirp (Figure 6). The features having the highest correlation with fitness (most correlated features (MCF)) are similar to the optimal pulses found by the GA search. The analysis does not expose any uncorrelated or "passenger" features. That is, the optimal pulse shapes do not contain much unnecessary structure.

Results of the analysis for one search in CHD in cyclohexane at $\tau = 12$ ns using broad bandwidth excitation pulses are shown in Figure 7. The two directions with the largest variance appear to roughly correspond to quadratic and cubic phase, respectively. They account for about one-third of the variance of the search and half of the phase profile of the optimal pulse. These directions also correlate better with fitness than other principal components. Quadratic phase is an important direction in the search. On the other hand, the most correlated feature resembles the best pulse and more significantly, the second principal

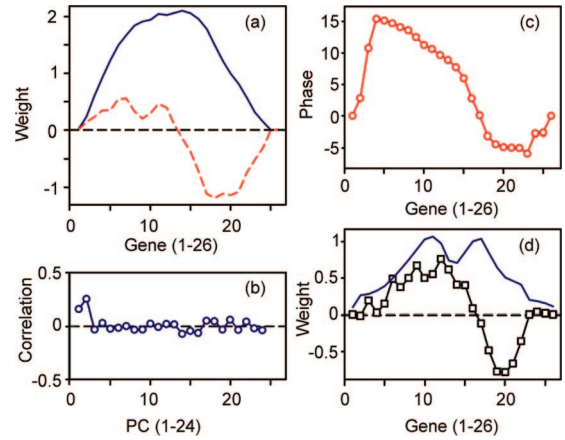

Figure 7. Analysis results for CHD in cyclohexane at $\tau = 12$ ns. (a) Phase profiles for the first (blue, solid) and second (red, dashed) principal components. (b) The correlation with fitness for all components illustrates the relative importance of the first two. (c) Phase profile of optimal pulse and (d) most correlated feature (black squares) for this search. The blue line in (d) is the spectral profile of the laser pulse. Gene 1 is the low-frequency, red edge of the spectrum.

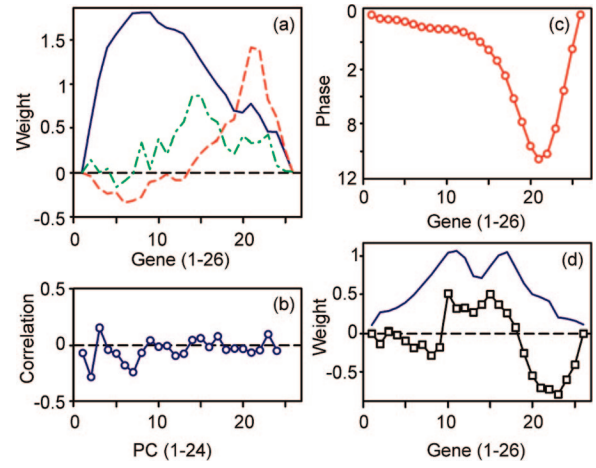

Figure 8. Analysis results for cyclohexane at $\tau = 12$ ns. (a) Phase profiles for the first (blue, solid), second (red, dashed), and third (green, dot-dash) principal components. (b) The correlation with fitness for all components illustrates that a number of the principal components contribute to the fitness. (c) Phase profile of optimal pulse and (d) most correlated feature (black squares) for this search. The blue line is the spectral profile of the laser pulse. Gene 1 is the low-frequency, red edge of the spectrum.

component in the PCA analysis. Consistent with the plots in Figure 5, quadratic phase contributes little to the most correlated feature despite its importance in the PCA analysis, whereas a significant cubic component is clearly identified.

When this analysis is applied to a GA search conducted in neat cyclohexane, a somewhat different conclusion emerges (Figure 8). Unlike the optimization of CHD in cyclohexane, in this search several of the principal components correlate with fitness, most significantly the second, third, sixth, and seventh components have high correlation with fitness. The phase profile of the optimal pulse most closely resembles the second principal component, but the most correlated feature is not well approximated by any of the principal components. Contrary to the conclusions from Figure 5, the most correlated feature for this search does not correlate with positive quadratic phase but is better approximated as a sum of even powers of phase, including a negative quadratic contribution and a positive quartic contribution. The second and third most correlated features (not

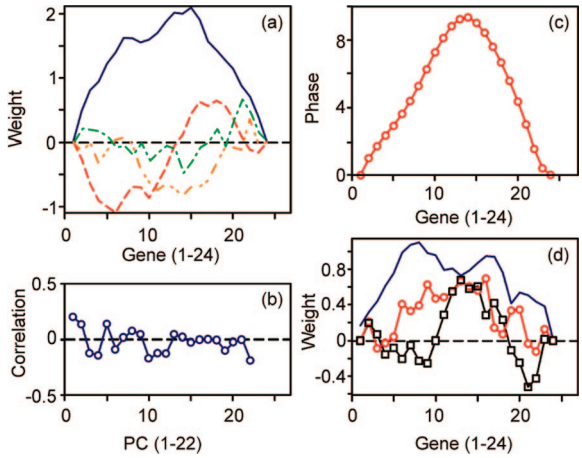

Figure 9. Analysis results for CHD in hexane at $\tau = 12$ ns. (a) Phase profiles for the first (blue, solid), second (red, dashed), third (green, dot-dash), and fourth (orange, dot-dot-dash) principal components. (b) The correlation with fitness for all components illustrates that many of the principal components contribute to the fitness. (c) Phase profile of optimal pulse and (d) Most correlated feature (black squares) and second most correlated feature (red circles) for this search. The blue line is the spectral profile of the laser pulse. Gene 1 is the low-frequency, red edge of the spectrum.

shown) are complex and not well modeled by a polynomial expansion, but do exhibit features consistent with a simple approximation by positive quadratic phase.

The statistical analysis of the GA search optimizing the formation of Z-HT from CHD in hexane is more complex (Figure 9). The first principal component and the phase profile of the optimal pulse both reflect a significant contribution from negative quadratic phase, in agreement with the analysis plotted in Figure 4. On the other hand, many of the principal components correlate with fitness. In this case the most correlated feature does not clearly resemble any of the principal components, or for that matter, the phase of the optimal pulse, suggesting that the optimal pulse may carry some passenger features. The second most correlated feature is well modeled by negative quadratic phase, suggesting that negative linear chirp does play a significant role, as expected from the plots in Figure 4. This analysis is also in agreement with the projection in Figure 4 that places the region of high fitness around zero cubic phase. Clearly, however, the pulse features responsible for the optimization of hexatriene formation are more complex than simple linear chirp.

IV. Discussion

Although detailed analysis of both optimal pulses and the correlation between pulse shape and fitness has helped elucidate optical control parameters, interpreting the control mechanisms in terms of the ring-opening dynamics remains a challenging task. Some insights may be gained by reviewing the application of optimal control theory to CHD and other photoisomerization reactions.

A. Comparison to Optimal Control Theory Results. Geppert and de Vivie-Riedle applied OCT to the ring-closure reaction (cZc-HT → CHD).[31,32] The optimal pulse consisted of two subpulses, corresponding to a pump−dump sequence. The complex "pump" pulse excites a wave packet on the S_2 PES with enough momentum to propagate directly toward the Franck−Condon (FC) region of the target (CHD). Once in the CHD FC region, a lower frequency "dump" pulse stimulates emission to the target state. Notably, the wave packet bypasses the conical intersections entirely. The authors explain that the all-optical pump−dump solution is faster and more effective than using the conical intersections.[31,32]

In a different study involving only the S_1 and S_0 PES, Geppert and de Vivie-Riedle demonstrated that the rate of the CHD ring-opening reaction can be controlled by forcing the wave packet to relax through the less efficient of two available S_1/S_0 conical intersections.[42] The optimal pulse was negatively chirped and the result utilized a pump-dump mechanism. In this case, however, the pulse consists of many pump-dump sequences within the CHD FC region. The initially excited wave packet gains momentum along the torsional reaction coordinate (the direction of steepest descent on the S_2 PES). When the wave packet is dumped, it experiences a negative gradient on the ground-state PES and slows down. The wave packet is progressively slowed by several pump-dump cycles, and consequently never gains enough momentum along the torsional coordinate to reach the higher energy more efficient conical intersection. Instead, the wave packet relaxes toward the targeted less efficient minimum energy conical intersection.

The reaction velocity study of Geppert et al.[42] underscores the role of wave packet momentum along the torsional reaction coordinate in the CHD isomerization. In our earlier work, we proposed that a ground-state wave packet could be generated by nonresonant impulsive excitation of low-frequency ground-state torsional modes. Time-resolved resonance Raman measurements show that σ-backbone is significantly involved in the nominally $\pi-\pi^*$ excitation, and the CHD relaxation initially involves the symmetric CH_2 twisting modes (1321 cm^{-1}), symmetric CH_2-CH_2 stretches, and low-frequency torsional modes.[33] Our narrowband experiments on CHD found that third-order phase resulted in a pulse train with a period of approximately 250 fs.[9] Although the pulse trains are slower than lowest frequency Raman modes of CHD, the period represents the most complex modulation attainable with the available optical bandwidth ($\Delta\nu = 125$ cm^{-1}).

A similar mechanism was identified in simulations controlling the cis−trans isomerization of retinal in rhodopsin.[52,53] In this system, the optimal pulse is highly structured with the majority of the pulse used to excite a ground-state wave packet along the reaction coordinate. This initial momentum helped maintain wave packet localization along the reaction coordinate when population was finally transferred to the excited state.[52] If the bulk of the pulse is spent preparing a high-momentum wave packet in the ground state, this could reconcile the fact that the duration of the optimal pulse found at the later pump-probe delay is longer than the CHD reaction time.

Besides creating a wave packet with large momentum along the torsional direction, a relevant control mechanism may be in creating a wave packet that will compensate for dispersion the wave packet experiences during field-free propagation on the S_1 excited state. For a wave packet propagating on an anharmonic PES, high-frequency components take longer to reach the outer turning point and begin to lag behind the lower frequency components. The situation of high-frequency components following low-frequency components is a positively chirped wave packet. If the vibrational wave packet is initially excited with a negative chirp, it will self-compress as it propagates.[54] Wave packet localization of this type was first proposed and demonstrated for a wave packet oscillating in a Morse potential.[54–56]

Wave packet localization at the conical intersections is thought to be important in CHD.[39] By controlling the position where the wave packet is localized, chirp can influence the wave

packet dynamics without directly guiding the wave packet to a conical intersection. Lee et al.[48] also considered wave packet localization as a possible mechanism in optimizing photoisomerization of the laser dye DCM. It is interesting that negative chirp is a common feature of the optimal pulses found in our CHD ring-opening and the DCM photoisomerization. In both molecules, the reaction proceeds through multiple electronic surfaces. The internal conversion mechanisms may also contribute dispersion,[57] e.g., high-energy components of the wave packet may pass through the conical intersection first. This possibility could be explored in more detail through quantum mechanical simulations.

The pulses in our experiments can represent only very limited control of the coherent wave packet on the short-lived S_2 state, although a non-zero cross section for three-photon excitation to the S_1 state may allow control on this longer-lived state.[29] The ground-state electronic configurations for both CHD and Z-HT are symmetric (designated 1A). The lowest lying singly excited singlet state in the FC region of each molecule is antisymmetric (designated 1B). $1A \rightarrow 1B$ is a $\pi-\pi^*$ transition. A second symmetric state (2A) has a diffuse and singly excited Rydberg 3s character in the FC region but is quickly stabilized as a doubly excited π^* orbital.[32,35] Hückel theory predicts three nearly degenerate doubly excited electronic configurations for the 2A state.[33] The strongly allowed $1A \rightarrow 1B$ transition carries 3−4 times more oscillator strength than the weakly allowed $1A \rightarrow 2A$ transition.[34,58] Accordingly, the S_1 state is usually considered to be "dark," though S_0-S_1 transitions are not symmetry forbidden. The energies of the 1B and 2A states differ by approximately 1 eV in the FC region.

B. Strong-Field Effects. A valid criticism of the multiphoton excitation of CHD concerns whether the strong-field excitation conditions perturb the excited-state structure. For the transform-limited pulses used in these experiments, the laser field approaches 0.3 V/Å. It is reasonable to suspect that fields of this strength cannot be treated as perturbative considering that field ionization can occur.[59] Such strong-field effects may positively contribute to solvent ionization or fragmentation processes responsible for the broad absorption spectrum optimized by nearly transform-limited pulses at the earlier time delay in either hexane or cyclohexane. On the other hand, the large linear chirp found optimal for CHD solutions reduces the average laser field strength to <0.07 V/Å, which is within the range of field strengths for which femtosecond multiphoton ionization in solvents can be treated as a perturbative phenomenon.[60] The GA optimization process could conceivably be driven to highly chirped pulses by a need to minimize the strong-field effects to obtain subtle control of the specific process of Z-HT formation. As discussed above, however, this mechanism alone does not explain the apparent preference for negative chirp.

Even within the perturbation limit, multiphoton processes may influence solvent photochemistry. Steady-state absorption measurements reported in our previous paper[9] showed that both CHD solution and neat solvent samples exhibited relatively strong absorption features that were photochemical in origin but were not due to Z-HT. Multiphoton photolysis studies on liquid alkanes have shown both multiphoton ionization (MPI) and excitation of subionization continuum states. The ionization potential of hexane is 10.13 eV,[61] so MPI would be a sixth- or seventh-order process. Fluorescence studies in liquid hexane excited via multiphoton excitation with 800 nm pulses suggest that MPI actually scales as the seventh or eighth power of the pulse intensity.[62] Following ionization, geminate electron-ion recombination occurs within 15 ps in hexane, leaving the molecule in the S_1 excited state.[63] High-energy subionization states (S_n) decay nonradiatively by fragmentation into neutral radicals and by internal conversion to the S_1 state.[62,63] The S_1 states of alkanes decay predominantly through decomposition by H_2 elimination.[63]

We also determined that 1,3,5-hexatriene could be made from cyclohexane, particularly if the sample volume was not refreshed between laser shots. Why HT was observed as a photofragment of cyclohexane but not of hexane is not entirely clear. Cyclohexane has a lower ionization potential (9.86 eV[61]) and tended to produce more deep UV photoproducts. 1,3-Cyclohexadiene has an even lower ionization potential (8.25 eV[64]) and CHD fragmentation may also contribute to the deep UV photoproducts. The formation of a CHD radical cation could also affect solvent photodegradation through hydrogen abstraction, as has been shown for perylene in hexane.[65] On the other hand, ionized CHD molecules that subsequently relax to the S_1 state through internal conversion may simply follow one of the reactive pathways on the S_1 PES. Internal conversion from subionization states in CHD reached through 4-photon absorption is a possible pathway to Z-HT; the dynamics of these higher order processes are not known. On the basis of intensity arguments, we expect the three-photon resonant isomerization will be the dominant reaction for CHD. These complications compounding CHD photochemistry with solvent fragmentation prevented the determination of absolute quantum yields for the multiphoton CHD → Z-HT reaction. However, the magnitude of the difference spectrum observed with transform-limited pulses suggests photoproduct formation on the order of 0.05% within the sample volume.

Recent studies of the photofragmentation of $CpMn(CO)_3$ are perhaps relevant to the CHD experiments described here.[66–68] In these experiments, and in the related theoretical analysis, nonresonant multiphoton transitions are used to control access to dissociation and ionization channels. The simulations demonstrate the efficacy of control of the position of the excited-state wavepacket with weak or intermediate field multiphoton excitation, within the limit of a perturbation theory approach.[68] The simulations do not include dephasing or decoherence.

V. Conclusions and Outlook

Several recent experiments, including the experiments discussed above, demonstrate that it is possible to use optical pulse shaping and multiphoton interactions to influence photoproduct formation in chemical systems. Using closed-loop feedback, learning algorithms are able to identify pulses that increased the desired target state. In our experiments formation of Z-HT was increased by as much as a factor of two over the transform-limited pulse. The genetic algorithm was also able to identify pulses that decreased solvent fragmentation, while leaving the formation of Z-HT essentially unaffected. The highest yields of Z-HT did not occur for the highest peak intensity laser pulses and did not conform to the I^3 power law expected of an incoherent process. Genetic algorithm searches consistently found that negative quadratic phase optimized Z-HT production.

From these experiments we conclude that extremely broadband coherent pulses are not required for multiphoton control of the CHD photoisomerization. We proposed involvement of low-frequency ground-state vibrational modes based on the observation that the nonlinear absorption of 800 nm light which leads to Z-HT formation is not dominated by the third-order

process required to reach the excited-state manifold. One potential mechanism maximizes the light−molecule interaction by vibrationally exciting the molecule in the ground state where the Franck−Condon region is bound. When the population is finally excited, additional momentum along the torsional coordinate may keep the wave packet localized as it moves toward the conical intersection. Localization could also precompensate for dispersion cause by the S_1 PES and possibly the S_2/S_1 conical intersection.

On a more general level, the results described here demonstrate the wealth of information available in a typical optical control experiment. Statistical analyses of data sets obtained in learning algorithm searches in neat cyclohexane and for CHD in hexane and cyclohexane highlighted the importance of linear and quadratic chirp, while demonstrating that the control features are not so easily defined. This analysis also distinguishes between well-defined and ill-defined fitness functions and search spaces. In any fitness-directed search the search sets do not represent random samplings of pulses. The bias in the search does not discredit statistical analysis but must be taken into account. It is also important to note that common pulse characteristics may be identified in a principal component analysis for systematic or experimental reasons unrelated to, or only marginally related to, the fitness goal of the experiment. The multivariate statistical analysis developed by Damrauer provides one approach to tackle this problem, reducing the multidimensional search space to a single control variable.[16,19] Fitness correlated analyses such as the MCF analysis described above provide additional approaches for robust identification of pulse features associated with formation of the desired target state.

Acknowledgment. This work has been supported the National Science Foundation through Grants Nos. 9987916, 0078972, 0718219, and the FOCUS Center at the University of Michigan.

References and Notes

(1) Mukamel, S. *Annu. Rev. Phys. Chem.* **2000**, *51*, 691–729.
(2) Brumer, P.; Shapiro, M. *Annu. Rev. Phys. Chem.* **1992**, *43*, 257–282.
(3) Weiner, A. M. *Rev. Sci. Instrum.* **2000**, *71*, 1929–1960.
(4) Hillegas, C. W.; Tull, J. X.; Goswami, D.; Strickland, D.; Warren, W. S. *Opt. Lett.* **1994**, *19*, 737–739.
(5) Rabitz, H. *Science* **2003**, *299*, 525–526.
(6) Kawashima, H.; M., W. M.; Nelson, K. A. *Annu. Rev. Phys. Chem.* **1995**, *46*, 627–656.
(7) Judson, R. S.; Rabitz, H. *Phys. Rev. Lett.* **1992**, *68*, 1500–1503.
(8) Kohler, B.; Krause, J. L.; Raksi, F.; Wilson, K. R.; Yakovlev, V. V.; Whitnell, R. M.; Yan, Y. *Acc. Chem. Res.* **1995**, *28*, 133–140.
(9) Carroll, E. C.; Pearson, B. J.; Florean, A. C.; Bucksbaum, P. H.; Sension, R. J. *J. Chem. Phys.* **2006**, *124*, 114506.
(10) Levis, R. J.; Rabitz, H. A. *J. Phys. Chem. A* **2002**, *106*, 6427–6444.
(11) Bardeen, C. J.; Yakovlev, V. V.; Wilson, K. R.; Carpenter, S. D.; Weber, P. M.; Warren, W. S. *Chem. Phys. Lett.* **1997**, *580*, 151–158.
(12) Assion, A.; Baumert, T.; Bergt, M.; Brixner, T.; Kiefer, B.; Seyfried, V.; Strehle, M.; Gerber, G. *Science* **1998**, *282*, 919–922.
(13) Pearson, B. J.; White, J. L.; Weinacht, T. C.; Bucksbaum, P. H. *Phys. Rev. A* **2001**, *63*, 063412.
(14) Cardoza, D.; Langhojer, F.; Trallero-Herrero, C.; Monti, O. L. A.; Weinacht, T. *Phys. Rev. A* **2004**, *70*, 053406.
(15) Cardoza, D.; Trallero-Herrero, C.; Langhojer, F.; Rabitz, H.; Weinacht, T. *J. Chem. Phys.* **2005**, *122*, 124306.
(16) Montgomery, M. A.; Meglen, R. R.; Damrauer, N. H. *J. Phys. Chem. A* **2006**, *110*, 6391–6394.
(17) Shane, J. C.; Lozovoy, V. V.; Dantus, M. *J. Phys. Chem. A* **2006**, *110*, 11388–11391.
(18) White, J. L.; Pearson, B. J.; Bucksbaum, P. H. *J. Phys. B* **2004**, *37*, L399–L405.
(19) Montgomery, M. A.; Meglen, R. R.; Damrauer, N. H. *J. Phys. Chem. A* **2007**, *111*, 5126–5129.
(20) Montgomery, M. A.; Damrauer, N. H. *J. Phys. Chem. A* **2007**, *111*, 1426–1433.
(21) White, J. L.; Pearson, B. J.;. Carroll, E. C.;. Florean, A. C.; Bucksbaum, P. H.; Sension, R. J. In *Femtochemistry VII: Fundamental Ultrafast Processes in Chemistry, Physics, and Biology*; Castleman, A. W., Jr., Kimble, M., Eds.; Elsevier: Amsterdam, 2006; pp 455−465.
(22) Laarhoven, W. H. In *Photochromism: Molecules and Systems*; Dürr, H., Bouas-Laurent, H., Eds.; Elsevier: Amsterdam, 2003; pp 270−313.
(23) Saltiel, J.; Sun, Y.-P. In *Photochromism molecules and systems*; Dürr, H. , Bouas-Laurent, H. , Eds.; Elsevier: Amsterdam, 2003; pp 64−164.
(24) Pullen, S.; Walker, L. A., II; Donovan, B.; Sension, R. J. *Chem. Phys. Lett.* **1995**, *242*, 415–420.
(25) Pullen, S. H.; Anderson, N. A.; Walker, L. A., II; Sension, R. J. *J. Chem. Phys.* **1998**, *108*, 556–563.
(26) Anderson, N. A.; Pullen, S. H.; Walker, L. A., II; Shiang, J. J.; Sension, R. J. *J. Phys. Chem. A* **1998**, *102*, 10588–10598.
(27) Lochbrunner, S.; Fuss, W.; Schmid, W. E.; Kompa, K.-L. *J. Phys. Chem. A* **1998**, *102*, 9334–9344.
(28) Fuss, W.; Hofer, T.; Hering, P.; Kompa, K. L.; Lochbrunner, S.; Schikarski, T.; Schmid, W. E. *J. Phys. Chem.* **1996**, *100*, 921–927.
(29) Anderson, N. A.; Sension, R. J. In *Liquid Dynamics Experiment, Simulation, and Theory*; Fourkas, J., Ed.; American Chemical Society: Washington, DC, 2002; pp 148−158.
(30) Anderson, N. A.; Shiang, J. J.; Sension, R. J. *J. Phys. Chem. A* **1999**, *103*, 10730–10736.
(31) Geppert, D.; Seyfarth, L.; de Vivie-Riedle, R. *Appl. Phys. B* **2004**, *79*, 987–992.
(32) Geppert, D.; de Vivie-Riedle, R. *J. Photochem. Photobiol. A* **2006**, *180*, 282–288.
(33) Trulson, M. O.; Dollinger, G. D.; Mathies, R. A. *J. Chem. Phys.* **1989**, *90*, 4274–4281.
(34) Tamura, H.; Nanbu, S.; Nakamura, H.; Ishida, T. *Chem. Phys. Lett.* **2005**, *401*, 487–491.
(35) Garavelli, M.; Page, C. S.; Celani, P.; Olivucci, M.; Schmid, W. E.; Trushin, S. A.; Fuss, W. *J. Phys. Chem. A* **2001**, *105*, 4458–4469.
(36) Celani, P.; Bernardi, F.; Robb, M. A.; Olivucci, M. *J. Phys. Chem.* **1996**, *100*, 19364–19366.
(37) Celani, P.; Ottani, S.; Olivucci, M.; Bernardi, F.; Robb, M. A. *J. Am. Chem. Soc.* **1994**, *116*, 10141–10151.
(38) Minnaard, N. G.; Havinga, E. *Recl. Trav. Chim. Pays-Bas.* **1973**, *92*, 1315–1320.
(39) Hofmann, A.; de Vivie-Riedle, R. *J. Chem. Phys.* **2000**, *112*, 5054–5059.
(40) Hofmann, A.; de Vivie-Riedle, R. *Chem. Phys. Lett.* **2001**, *346*, 299–304.
(41) Hofmann, A.; Kurtz, L.; de Vivie-Riedle, R. *Appl. Phys. B* **2000**, *71*, 391–396.
(42) Geppert, D.; de Vivie-Riedle, R. *Chem. Phys. Lett.* **2005**, *404*, 289–295.
(43) de Vivie-Riedle, R.; Kurtz, L.; Hofmann, A. *Pure Appl. Chem.* **2001**, *73*, 525–528.
(44) Dugan, M. A.; Tull, J. X.; Warren, W. S. *J. Opt. Soc. Am. B* **1997**, *14*, 2348–2358.
(45) Henry, E. R.; Hofrichter, J. *Methods Enzymol.* **1992**, *210*, 129–192.
(46) Brixner, T.; Damrauer, N. H.; Niklaus, P.; Gerber, G. *Nature* **2001**, *414*, 57–60.
(47) Brixner, T.; Damrauer, N. H.; Kiefer, B.; Gerber, G. *J. Chem. Phys.* **2003**, *118*, 3692–3701.
(48) Lee, S.-H.; Jung, K.-H.; Sung, J. H.; Hong, K.-H.; Nam, C. H. *J. Chem. Phys.* **2002**, *117*, 9858–9861.
(49) Meshulach, D.; Silberberg, Y. *Nature* **1998**, *396*, 239.
(50) Lozovoy, V. V.; Pastirk, I.; Walowicz, K. A.; Dantus, M. *J. Chem. Phys.* **2003**, *118*, 3187–3196.
(51) Jolliffe, I. T. *Principal Component Analysis*, 2nd ed.; Springer: Berlin, 2002.
(52) Abe, M.; Ohtsuki, Y.; Fujimura, Y.; Domcke, W. *J. Chem. Phys.* **2005**, *123*, 144508.
(53) Ohtsuki, Y.; Ohara, K.; Abe, M.; Nakagami, K.; Fujimura, Y. *Chem. Phys. Lett.* **2003**, *369*, 525–533.
(54) Kohler, B.; Krause, J. L.; Raksi, F.; Rose-Petruck, C.; Whitnell, R. M.; Wilson, K. R.; Yakovlev, V. V.; Yan, Y.; Mukamel, S. *J. Phys. Chem.* **1993**, *97*, 12602–12608.
(55) Krause, J. L.; Whitnell, R. M.; Wilson, K. R.; Yan, Y.; Mukamel, S. *J. Chem. Phys.* **1993**, *99*, 6562–6578.
(56) Cao, J.; Wilson, K. R. *J. Chem. Phys.* **1997**, *107*, 1441–1450.
(57) Piryantinski, A.; Stepanov, M.; Tretiak, S.; Chernyak, V. *Phys. Rev. Lett.* **2005**, *95*, 223001.
(58) Share, P. E.; Kompa, K. L.; Peyerimhoff, S. D.; van Hemert, M. C. *Chem. Phys.* **1988**, *120*, 411–419.
(59) DeWitt, M. J.; Levis, R. J. *Phys. Rev. Lett.* **1998**, *81*, 5101–5104.

(60) Greever, J. S.; Turner, J. B. M.; Kauffman, J. F. *J. Phys. Chem. A* **2001**, *105*, 8635–8641.

(61) Castillejo, M.; Couris, S.; Koudoumas, E.; Martin, M. *Chem. Phys. Lett.* **1999**, *308*, 373–380.

(62) Volkmer, A.; Wynne, K.; Birch, D. J. S. *Chem. Phys. Lett.* **1999**, *299*, 395–402.

(63) Sander, M. U.; Brummund, U.; Luther, K.; Troe, J. *J. Phys. Chem.* **1993**, *97*, 8378–8383.

(64) Harada, H.; Shimizu, S.; Yatsuhashi, T.; Sakabe, S.; Izawa, Y.; Nakashima, N. *Chem. Phys. Lett* **2001**, *342*, 563–570.

(65) Greever, J. S.; Turner, J. B. M.; Kauffman, J. F. *J. Phys. Chem. A* **2003**, *107*, 4072–4080.

(66) Daniel, C.; Full, J.; Gonzalez, L.; Kaposta, C.; Krenz, M.; Lupulescu, C.; Manz, J.; Minemoto, S.; Oppel, M.; Rosendo-Francisco, P.; Vajda, S.; Woste, L. *Chem. Phys.* **2001**, *267*, 247–260.

(67) Ambrosek, D.; Oppel, M.; Gonzalez, L.; May, V. *Chem. Phys. Lett.* **2003**, *380*, 536–541.

(68) Ambrosek, D.; Oppel, M.; Gonzalez, L.; May, V. *Opt. Commun.* **2006**, *264*, 502–510.

JP8013404